PedPIV: Pedestrian Velocity Extraction From Particle Image Velocimetry

Muhammad Baqui and Rainald Löhner

***Abstract*— The analysis of velocities from high-density pedestrian events may provide more information on pedestrian flow dynamics. A framework based on particle image velocimetry (PIV)—a technique commonly used in experimental fluid dynamics—has been developed to evaluate the pedestrian velocities from high-density pedestrian events. The framework takes a sequence of two or more images from a regular closed-circuit television camera and obtains the flow properties (speed, direction) of the pedestrians. A detailed analysis has been done in both the qualitative and quantitative aspects of adapting PIV to pedestrian flow. An investigation through the use of the fundamental diagram and real-time extraction of crowd velocities is also presented and discussed. The proposed PIV-based framework enables on-the-spot analysis of pedestrian flow via velocity extraction in a reliable, automated manner.**

***Index Terms*— High density pedestrian flow, crowds management, pedestrian traffic management, particle image velocimetry, pedestrian traffic planning.**

I. Introduction

PEDESTRIAN transport or pedestrian flow has become an important part of multi-modal transportation systems. Recent studies undertaken by Baek *et al.* [1], Oliveira *et al.* [2] and Li *et al.* [3] investigated different pedestrian detection techniques that can help in predicting congestion buildup and thus avoiding accidents. Detecting or counting pedestrians enables one to get the quantitative measure of density. Density and velocity are fundamental properties of pedestrian flow. Given that dangerous crowd situations usually arise when densities are high [4], [5], it is important to analyze pedestrian velocities in such a setting. Conducting controlled experiments with high density crowds is risky as it could trigger accidents. It is for this reason that, with a few exceptions (e.g. [6], [7]) the data for high density crowds is sparse. The current work offers a convenient way of studying pedestrian velocities through the Particle Image Velocimetry (PIV) technique. PIV is a widely used technique in experimental fluid dynamics. Along with velocity, PIV can also provide other flow properties such as streamlines, vorticity and turbulence. PIV also has lower processing times as compared to other techniques such as Optical flow [8], [9]. There has been a very limited number of studies applying the PIV technique for crowd velocity extraction. Studies of this kind can be found in the works of Jiayue *et al.* [10], Ma *et al.* [11], and, Zhang *et al.* [12]. These works rely on fixed grid for perspective correction, which limits the scope of application as it requires extensive manual intervention. These studies also do not explore the accuracy and uncertainty of PIV velocities for crowd images in depth. This paper undertakes a thorough investigation on estimating the measurement uncertainty and sensitivity of the PIV method with crowd images.

The paper is organized as follows. In section II the current state of the research and development with PIV and empirical studies of crowds analysis are discussed. Section III describes the PIV theory. Section IV performs a qualitative and quantitative analysis of the feasibility of PIV for the present purpose. In section V, results are shown for the pedestrian velocities obtained from PIV analysis of crowd images. Section VI draws the conclusion of this work.

II. Background

A. Particle Image Velocimetry

PIV was developed in the 1980s. The foundational works were performed by Adrian et al. [13], [14], Willert and Gharib [15], Keane and Adrian [16]. The development of digital image acquisition (DPIV) techniques provided a breakthrough in PIV application and triggered the potential of its widespread use afterwards. Continuous research and development over the next two decades has resulted in establishing it as one of the the primary tools for evaluation of experimental fluid flow. At present, one can find stereoscopic, iterative, and adaptive methods of PIV [17], [18]. The main method for PIV particle tracing is statistical cross correlation. Cross correlation can be obtained in spatial domain or in frequency domain. Other methods for obtaining correlation can be found in the works of Scarano [19] and Thomas *et al.* [20].

The traditional application area of PIV is experimental aerodynamics. Baqui and Mahmud [21], [22] have used PIV to measure the performance of an aerodynamic flow separation control device. Recently, PIV algorithms have been applied to many areas within and outside of fluid dynamics, e.g. metal fatigue experiments (Vanlanduit *et al.* [23]), water waves (Cowen and Sveen [24]), audio speaker performance (Rossi *et al.* [25], to name a few. Due to its widespread use and popularity, both commercial and open source packages are available for PIV analysis. PIVlab [26], Matpiv [27] and

Manuscript received September 27, 2017; revised March 10, 2018, August 7, 2018 and December 18, 2018; accepted January 31, 2019. The Associate Editor for this paper was A. Hegyi. *(Corresponding author: Muhammad Baqui.)*

M. Baqui is with the Department of Computational and Data Science, George Mason University, Fairfax, VA 22030 USA (e-mail: mbaqui@gmu.edu).

R. Löhner is with the School of Computational Sciences, George Mason University, Fairfax, VA 22030 USA (e-mail: rlohner@gmu.edu).

Digital Object Identifier 10.1109/TITS.2019.2899072

OpenPIV [28] are commonly used open source PIV packages. The current work has greatly benefited from and has been influenced by these packages.

B. Experimental Pedestrian Flow Measurements

Pedestrian flow analysis is an important area for transportation research and urban planning. There are a number of experimental studies that focus on pedestrian flow analysis at different levels of pedestrian densities. Among data collection techniques, video and image data collection are the most popular. By analyzing these data important conclusions are derived. Many experiments observe the change in fundamental properties by varying environmental settings (i.e. size, angle of walking corridor, room size etc.). One comprehensive study on designing pedestrian facilities was done by Predtechenskii and Milinskii [29], a relatively old work in which the authors carefully outlined design attributes for various density foot traffic facilities. Another big source of experimental data is Fruin [30]. Schadschneider *et al.* [31] discussed various properties of high density flows such as lane formation, density waves, oscillations etc. from a theoretical and experimental point of view. Some recent experimental studies can be found in Kretz *et al.* [32] and Helbing *et al.* [33]. Other works have focused on understanding the walking behavior of people through experimental and statistical analysis [34]–[36].

Boltes *et al.* [37] studied the parameters that govern the quality of pedestrian data extraction from video. For that purpose, errors due to perspective distortion, use of markers, type of markers, and other conditions were scrutinized in detail.

Ziemer *et al.* [38] performed an empirical study on pedestrian congestion in one dimensional motion with a periodic boundary condition. The fundamental diagram is also studied with various densities that result in stop-and-go waves. Yuan *et al.* [39] constructed a crowds monitoring system that is based on the real-time data collection from WiFi sensor, GPS tracker and video. In their work they highlight the need for proper calibration of camera in order to obtain accurate velocity information.

Daamen [40] presented SimPed, an operational tool to support designers of public transport facilities. The work also consist of experimental evaluations of walking behaviour, identification of critical flow parameters, modeling pedestrian behaviour and finally validation and verification of the model.

A particular work of Hoogendoorn *et al.* [41] discusses an approach to extract individual pedestrian data from digital video footage. The video data was collected during a large scale walking experiment involving around 80 volunteers. The data can be used for pedestrian simulation models to calibrate parameters and validation and verification of the model.

Khan *et al.* [42] constructed an algorithm for the automated detection of starting points, dominant motion and ending points of pedestrians from videos. Starting points are called sources and ending points are called sinks. The procedure used optical flow features to identify sources, sinks and dominant motion from video data.

Ettehadieh *et al.* [43] proposed an evolutionary algorithm for performance enhancement for tracking pedestrians from video data. With the simulated annealing based evolutionary algorithm, the performance of feature based trackers can be improved. Corbetta *et al.* [44] used an overhead kinetic (Kinect) sensor and automatic pedestrian tracking algorithm to record movement data of Eindhoven train station. The benefit of kinetic sensor is that it gives 3D information of pedestrians in the domain. Several interesting conclusions about walking behaviour, speed were made for bi-directional streams. Zhao *et al.* [45] performed experimental study of formation of pedestrian groups and their walking behaviour as groups. Kogler *et al.* [46] investigated how crowd behaviour changes over the years before and after a public event and how it impacted a public transport system in Vienna, Austria. Klüpfel [47] focused on incorporating various empirical parameters on the model to improve accuracy.

The experimental works to date measured mostly low to moderate density crowds. This is not surprising, as there is a significant amount of risk involved in performing experiments with high density pedestrian flow. However, from the operational point of view it is very important to understand high density pedestrian flow in order to avoid potential hazardous situations. The current framework provides an ideal platform to analyze such flows in automated manner.

C. Image Based Crowds Analysis

Crowd density estimation or crowd counting from an image is done with both regular images [48] and video images [49]. Video data is essentially a sequence of images. The benefit of video data is that it can provide the crowd movement or velocity information. Velocity is a fundamental information for any pedestrian flow analysis. Video based techniques have been applied recently to perform critical analysis of crowd disasters [50], [51]. The video based works mostly use the optical flow method in order to obtain velocity information. The optical flow equation is shown in equation 1

$$\frac{dI}{dt}(\vec{x}(t),t) = \frac{\partial I}{\partial t} + \frac{\partial I}{\partial x}\frac{dx}{dt} + \frac{\partial I}{\partial y}\frac{dy}{dt} = \nabla I\vec{u} + \frac{\partial I}{\partial t} \quad (1)$$

Here, $\vec{I}$ stands for the intensity of the image and $\vec{u}$ is the velocity. There are two unknowns, i.e. the velocities in x and y direction and one equation. The solution is obtained following a least squares approximation. The optical flow algorithm was first proposed by Horn and Schunck [8]. It considers a brightness constancy assumption between the frames. The assumption considers that there is no change in brightness between the two successive frames. An alternative algorithm for optical flow was proposed by Lucas and Kanade [9]. It is based on developing an iterative method to solve the equation with good initial values. Optical flow methods are also used to understand fluid flow. A detailed analysis of optical flow for fluid dynamics can be found in the work of Liu and Shen [52].

III. PIV Theory

In this section, the theoretical formulation of PIV technique is discussed within the realm of crowd image processing.

A PIV system for fluid flow consists of four main components: seeding particles, flow illumination device, frame grabber (camera) and image processing algorithm. For crowds, only the PIV Image processing algorithm is used. Image processing consists of two main components: cross correlation based pattern matching and sub pixel velocity estimation. These are discussed in the following sections.

A. Pattern Matching

The first step in the PIV image processing is the pattern matching through cross correlation. Cross correlation computes component-wise the inner product between the two input signals (images A and B in equation 2) and in this way obtains the maximum similarity. These signals are assumed to be very similar (ideally identical) and separated by a small timegap. For convenience, the input images are divided into smaller windows called interrogation spots. In equation 2, m × n correspond to the dimension of this interrogation spot. The result of the multiplication is stored in C, which is called the correlation surface. The same correlation can be obtained with the convolution of the signals in the Fourier domain (taking into accout that signal B need to be flipped). The convolution based cross correlation (equation 4) offers faster processing time: $O(n^2\ logm)$, compared to $O(n^2\ m^2)$.

$\forall i$ in m, j in n,

$$|A-B|^2 = A^2 + B^2 - 2AB \tag{2}$$

$$C(i,j) = \sum_k^m \sum_l^n A(k,l)B(i-k, j-l) \tag{3}$$

$$C(i,j) = IFFT(FFT(A(k,l)) * FFT(B(k,l))) \tag{4}$$

$$= \sum_k^m \sum_l^n A(k,l)B(k-i, l-j) \tag{5}$$

A typical correlation surface will have a distinct peak at the center and subsequent neighboring peaks in the vicinity of the peak.

B. Displacement Estimation

The peak of the correlation surface corresponds to the displacement experienced by the signal. In order to obtain the displacement at sub-pixel level accuracy, an interpolation is performed with the tallest peak (maximum value of the correlation surface) and its neighboring pixels [14]. This interpolation is performed by fitting a 3 point Gaussian as shown in the following. Let $P(i, j)$ be the pixel having the maximum of value of the correlation surface. Then, for sub-pixel accurate displacement, the Gaussian would take the form as presented in equation 6.

$$P_{i,j} = \frac{ln\ P_{i+1,j} - ln\ P_{i-1,j}}{2\ (2\ ln\ P_{i,j} - ln\ P_{i+1,j} - ln\ P_{i-1,j})} \tag{6}$$

The same equation is used for sub-pixel displacement along the $ythe$ axis, except now the j index is varied. Once the particle displacements are determined, the velocities can be obtained from equation 7, where s is the displacement and t the time.

$$v = \delta s/\delta t, s = [\delta x, \delta y] \tag{7}$$

Algorithm 1 Cross Correlation Velocity

```
Input : Image A and B, spot size m_x,m_y, overlap
Output: Velocity vectors: u and v
for window loop imsizex do
  for window to imsizey do
    W_a = Extract window from image A
    W_b = Extract window from image B
    W_b = Flip W_b upside down
    a1=FFT(W_a)
    b1=FFT(W_b)
    c1=a1*b1
    c=IFFT(c1)
    for indices in c do
      peakx=fit gaussian between i,i+1,i-1
      peaky=fit gaussian between j,j+1,j-1
      u=(window index-peakx)*scale
      v=(window index-peaky)*scale
    end for
  end for
end for
```

The velocity extraction process can be summarized with the following pseudocode:

C. Background Removal

In processing crowd images a common issue is the automatic identification and removal of the image background. For PIV studies in fluid dynamics, a mask is manually put along the stationary object (background). Here, an automated background removal based on color histogram threshold has been applied. Representative sections of the background are collected. Afterward, the color histogram between the input image and background section is compared based on the chi-squared distance [53] using equation 8.

$$d = 2 \sum \frac{(x_i - y_i)^2}{x_i + y_i} \tag{8}$$

The equation calculates a value d from x (input image) and y (background). If the value of d exceeds a pre-determined threshold (typically 0.84) then it is considered as background and a mask is put. The vectors after this background removal process can be seen in Figure 5.

D. Correction of Perspective

In almost all cases of pedestrian flows, the camera is not orthogonal to the flow, i.e. some amount of angle is always present in the image. The main contribution of this angle to the flow is that it exaggerates or shrinks the magnitude of the crowd movement. For example in Figure 6, the persons residing on the top portion of the image would experience a lesser amount of pixel movement compared to the ones residing in the bottom section. However, from a physical point of view, both persons should have similar velocities. The correction of perspective would also enable to obtain PIV displacements in real world units (e.g. meters).

The methodology employed here for the correction of perspective is based on the pinhole camera model and projective geometry. There are three different coordinate systems involved in this process. The 3D world coordinate, the 3D camera coordinate and the 2D image coordinate system. First, the camera intrinsic and extrinsic parameters are determined. Afterwards, an equation for a plane is constructed in the camera coordinate system from the landmark points. For these landmark points, the image coordinates and world coordinates are known. From the pin-hole camera model, all rays originate in the optical center. So in order to project a pixel into world coordinate center, all is needed is to find the intersection point of the line (constructed by optical center and the pixel) and the plane. Details of the method can be found in the [54].

IV. PIV Performance Characterization for Crowd Processing

In this section, numerical experiments are performed with time lapse crowd photos to explore the feasibility of the PIV technique for crowd velocity extraction. First, the datasets on which the experiments are performed are explained. Afterwards, in sections IV-B, IV-C the qualitative and quantitative performances are discussed.

A. Dataset Description

The present study focuses on evaluating PIV performance in velocity extraction of a high density pedestrian event: the Hajj. The Hajj is an interesting event for analyzing high density situations. High density of pedestrians give rise to stop-and-go waves, density waves, intersecting flows and in some cases crowd turbulence. To study the event carefully, three sets of time lapse photos were made available to the authors. These photos are collected from the CCTV cameras located at the Grand Mosque of Mecca. In Figure 1, a single frame from each of the images is presented. The first image [Figure 1(a)] is an example of a low density flow and low resolution (1920×1080 pixels) image. The second image [Figure 1(b)] is an example of a high density flow and high resolution (5760×3840 pixels) image. The third one [Figure 1(c)] represents a case for a low density flow and high resolution (5760×3840 pixels) image. Each image was captured from a different camera on the premise.

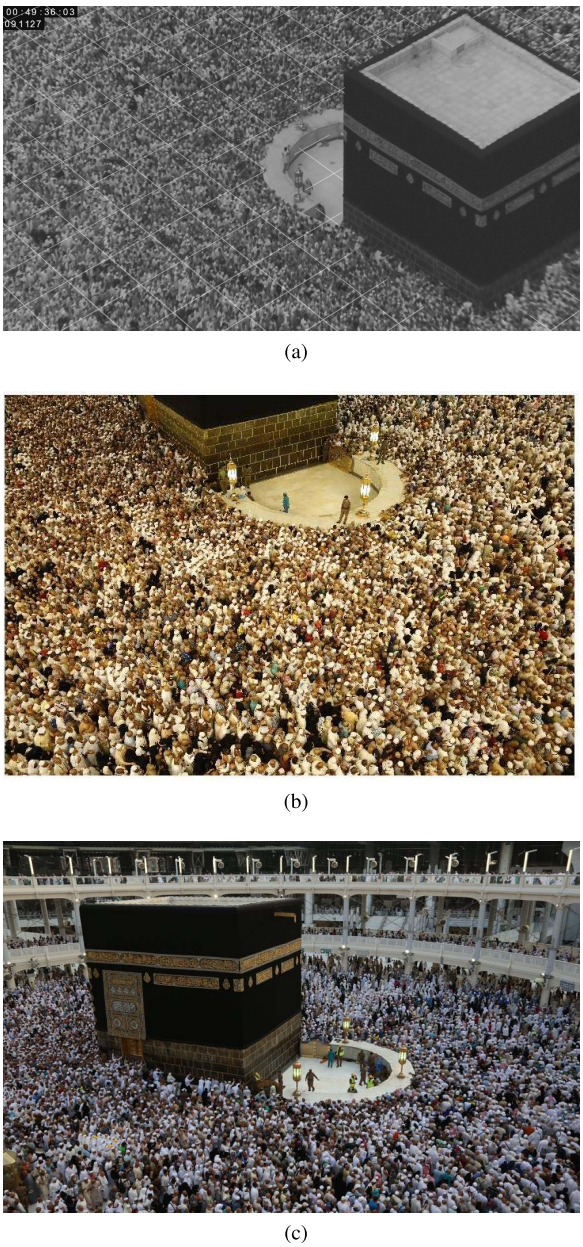

(a)

(b)

(c)

Fig. 1. A sample frame of the dataset. (a) First set. (b) Second set. (c) Third set.

B. Qualitative Analysis

One assumption for PIV correlation is that the motion of fluid particles needs to be uniform between the frames. The nonuniform motion would broaden the intensity peak and produce erroneous results. For PIV of fluids Charge Coupled Device (CCD) cameras are used. They have very high frame rate so they can capture uniform motion between the frames. Also, fluid motion does not vary in all directions. Unfortunately, for crowds movement such properties do not hold. Every human being walks at a different speed, and the direction of movement is also not uniform. Moreover, crowd images are mostly captured by overhead CCTV cameras or in some cases by regular digital cameras. The frame rate is not very high. Despite all these limitations, the correlation surface obtained from crowd images has been reliably able to produce displacement peaks. In Figure 2 the correlation surface with a spot size of 40×40 pixels is shown. The highest peak is found right at the center. Other peaks distributed almost uniformly distributed throughout the spatial domain.

The crowd images are taken in diverse settings. Poor illumination, presence of background and presence of perspective can deteriorate the image quality further. When crowd density is low it is not uncommon to have a nonmoving background scattered throughout the image. This is the reason why exploring the shape of correlation surface with background is important. In Figure 3 a background with a sharp variance

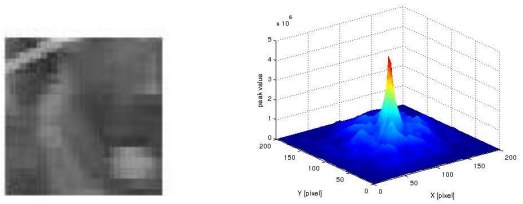

(a) (b)

Fig. 2. PIV correlation at spot size 40×40 pixels. (a) First input image. (b) correlation surface. The single distinct peak at the center.

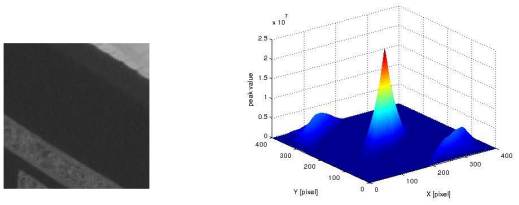

(a) (b)

Fig. 3. Correlation surface of a background component. The shape of the correlation surface is flat, very different from the ones presented earlier. These are examples of bad correlations.

in intensity and corresponding correlation surface is presented. The peak is not sharp but flat which is an indication of poor correlation. A poor correlation will result in spurious velocity vectors.

C. Quantitative Performance

In the previous section, qualitative aspects of PIV processing of crowd images were explored in the form of the shape of the correlation surface. The aim of the current section is to quantifiably measure the accuracy and uncertainty of PIV processing. In section IV-C.1 uncertainty estimation is explained. In section IV-C.2 measurements of PIV displacements are compared with ground truth countings. Finally, in section IV-C.3 the relation between correlation miss and PIV accuracy is explained.

1) Uncertainty Estimation: There are a number of ways to estimate the PIV uncertainty [55], [56]. Some of these methods are based on the cross correlation peak ratio [57]–[59], which is the ratio of highest peak to the second highest peak of the correlation surface. This ratio is also known as signal to noise ratio. When the signal to noise ratio is higher than 2.0 the main peak is considered to be of good quality [59]. For the crowd images analyzed here, the signal to noise ratio was always found to be higher than 2.0, except in the regions where a static background is present. Thorough quantification of the PIV uncertainty using the signal to noise ratio for crowd images proved unfeasible due to a number of issues. The empirical equation formed from the signal to noise ratio is mainly dependent on fluid particle diameter, seeding density, spot size etc. These quantities are not available with crowd images. Although a spot size is present, its value size is considerably higher than that encountered for PIV of fluid particles. Considering all these limitations, the method outlined by Sciacchitano et al. [60] was deemed most suitable for the current analysis.

Uncertainty quantification through image matching developed by Scicchitano *et al.* [60] relies on a statistical technique to estimate the measurement uncertainty of PIV. It operates in three stages: (a) Image matching of particle pairs, (b) Disparity vector construction from the matched pairs, and (c) Estimation of error from disparity vector ensemble.

a) Image matching of particle pairs: Let A and B be two images separated by a time difference δt. One image is taken as a reference pattern and the subsequent one is subjected to a transformation that minimizes the distance following an L-2 norm (similar to spatial cross correlation). A set of particles or feature points is tracked in order to quantify the matching. For crowd images no 'particles' are present. In order to circumvent this limitation, edges or corners (i.e. locations where the image gradient is high) are used instead. Of the many possible techniques, so-called Harris corners [61] were detected and tracked for two subsequent images.

b) Disparity vector construction: The disparity vector is computed from the spatial differences between the matched pairs.

$$D = [(a_1 - b_1), (a_2 - b_2), \ldots, (a_N - b_N)] \tag{9}$$

c) Statistical analysis of disparity vector ensemble: The statistical of measurement uncertainty outlined by Taylor and Kuyatt [62] indicates the relation between standard deviation to random error can be estimated as $\sigma/\sqrt{N}$. Here the quantity of interest is the disparity vector of the matched pairs. It is assumed for the sake of simplicity that the individual components of the disparity set are statistically independent and follow a Gaussian distribution. Hence, the RMS PIV error can be estimated as $\delta = \sigma/\sqrt{N}$. The expanded uncertainty U can also be estimated from a known value of the coverage factor k from the relation $U = k \cdot \delta$. The value of k will depend on the requirement from the user. Typically it is chosen as $k = 2$.

With the method outlined above, the uncertainty for PIV processing with crowd images can be readily determined. It will also give an estimate of error bounds for PIV correlation. In order to characterize the PIV error in different operating conditions, the three key PIV operating parameters (a) pixel displacement, (b) spot size and (c) particle density were investigated. The results are presented below:

d) Pixel displacement: The results for PIV error with respect to pixel displacements can be seen in Table I. For each dataset three different pixel displacements and their corresponding errors were determined. It can be seen that a higher amount of error was present for the first dataset. This was due to poor image quality. Note also that as the displacement values are increased a modest increase in the errors is observed.

e) Spot size: The effect of a gradual change in spot size on the PIV error is observed. Three different spot sizes were studied. The results are summarized in Table II. The noisy images of the first set again led to higher errors as compared to the other two datasets. A trial and error approach was employed for choosing the spot sizes. This is also common practice in fluid dynamics. The width of a person in the frame

TABLE I
PIV DISPLACEMENTS WITH ERROR

Dataset	Displacement (pixel)	Error magnitude (pixel)
1	26.3545	2.7332
1	26.7778	3.0719
1	27.8394	5.9670
2	34.6090	0.0758
2	35.9882	0.0790
2	37.1425	0.0796
3	51.2730	0.1694
3	58.1656	0.1949
3	59.6523	0.2050

TABLE II
PIV SPOTSIZE WITH ERROR

Dataset	Spot size (pixel)	Error magnitude (pixel)
1	60x60	2.8321
1	90x90	0.3773
1	120x120	0.2581
2	120x120	0.0557
2	150x150	0.0758
2	180x180	0.1179
3	120x120	0.1098
3	150x150	0.1694
3	180x180	0.2836

TABLE III
PIV PARTICLE DENSITY WITH ERROR

Dataset	Density	Error magnitude (pixel)
1	100	2.75
1	150	2.75
1	200	2.75
2	100	0.1123
2	150	0.0885
2	200	0.0758
3	100	0.2755
3	150	0.2057
3	200	0.1694

and the expected mean pedestrian velocity are considered when choosing the spot size. For the first set 60×60, 90×90 and 120×120 pixels spot sizes were investigated. For the remaining two datasets, 120×120, 150×150 and 180×180 pixels spot sizes were chosen. As can be seen in Table II, which summarizes the results, a clear optimium spot size can be identified.

f) Density: The final variable considered for PIV error characterization is density. This density is not the pedestrian density. It is the number of interest points/Harris corners present in the image. The performance of PIV depends on how well the algorithm can track the image features between the frames.Table III summarized the results. Note that for the second and third dataset choosing a higher number of interest points leads to a decrease in error. However, for the first set, an increase in the number of interest points did not produce any marked change in the error. This is due to the poor image quality of this dataset. The interest points identified were not sharp enough to be tracked.

TABLE IV
PIV PARTICLE DENSITY WITH ERROR

True Δx [pixel]	Measured Δx [pixel]	True Δy [pixel]	Measured Δy [pixel]	% Error
-3	-2.52	3	2.73	12.43
-3	-3.89	5	4.08	3.32
-8	-6.87	3	2.39	14.86
-5	-4.28	4	4.14	7.08
4	3.08	-2	-2.14	6.13
8	7.55	2	1.72	6.09

The PIV errors seen here for crowd images are about an order of magnitude higher than those obtained in experimental fluid dynamics (i.e. Sciacchitano *et al.* [60]). The main reason is that for fluid flow the colors are clearly defined and the laser sheet can be made very thin. In crowd images, the colors vary much more. Furthermore, shadowing as well as pedestrians turning and occluding each other leads to a higher degree of noise and uncertainty. Nevertheless, the pedestrian velocities obtained are in good agreement with other studies (see section V-B).

2) Measurement of Accuracy: The displacements obtained by PIV processing are also compared with ground truth movements. These are obtained by tracking manually the displacements of randomly selected pedestrians between two image frames, and comparing them to PIV displacements. Six random locations, listed in table IV, were considered.

One can see the close resemblance between the PIV and manually counted displacements for the majority of the data. The influence of noise in PIV measurements can be seen in the first and third entries of the table. Here, poor illumination resulted in an elliptically shaped peak that deteriorated the correlation output.

3) Correlation Miss: People move in all sorts of directions. There are circular patterns, intersecting or crossflow patterns, uniform flow at entrances, etc. For successfull correlation with PIV, interrogation spot size plays a major role. Specially in challenging situations such as in cross/intersecting flows, special attention must be given in selecting the proper spot size. When the spot size is not optimal, it will result in a large number of correlation misses. A correlation miss can be interprated as the PIV algorithm failing to produce any displacement value. When selecting the spot size, the dimension of the spot window should be at least 4 times higher than the maximum displacement experienced by the signal. For case of crowds moving at walking speed (i.e. 1.2 m/s), the spot size should be big enough so that most pedestrians stay between frame A and B. Moreover, it is always beneficial to keep some overlap (20-60%) between the frames. In the case when the maximum signal displacement is not known beforehand, it is safe to start with a bigger spot size and then gradually lower the spot size to an acceptable/optimal size. This is a design issue of the PIV algorithm. Even in fluid dynamics applications, the experimentalist has to do a number of trials in order to get to an optimal spot size. This issue can be further explained with the help of the log-log plot shown in Figure 4, which shows the number of correlation misses occurred for a given spot size. It can be seen that the number of misses

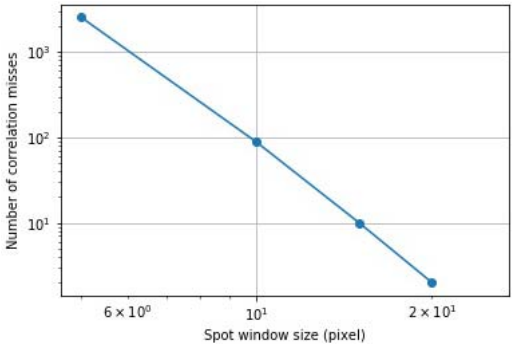

Fig. 4. Correlation miss for different spot sizes. An increase in spot size leads to a decrease in correlation misses. For spot sizes higher than 20×20 pixels no correlation miss was found.

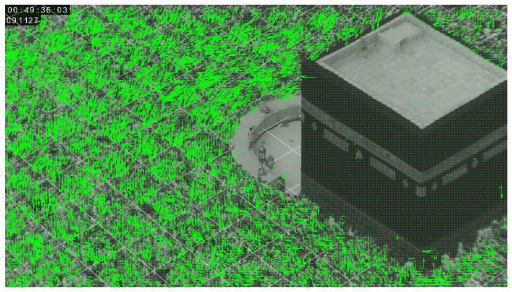

(a)

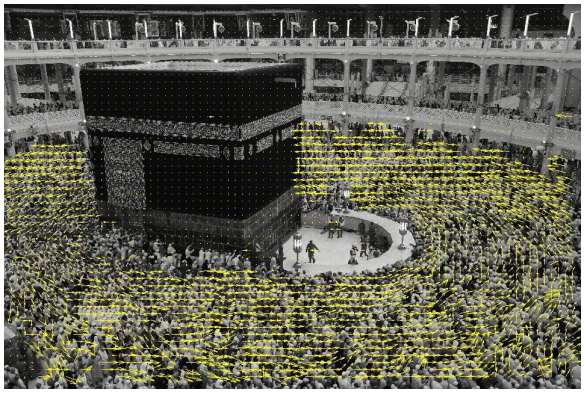

(b)

Fig. 5. Velocity vectors from datasets. (a) Sample vectors of dataset 1 after PIV. (b) Sample vectors of dataset 3.

decay exponentially to zero as the spot size is changed from very small to acceptable.

V. Results on Velocity Extraction

In the previous sections, qualitative and quantitative analyses of the PIV errors in crowd images have been presented. In this section, results are presented for pedestrian velocities from PIV processing.

In Figure 5 the velocity vectors obtained for the first and second set are presented. The vectors indicate a predominant circulatory motion. These two sets represent crowd images with moderate density (4-6 persons per sqm). It is also evident that the automatic background subtraction has been able to eliminate spurious vectors from the stationary components of the image. For PIV processing the spot size chosen were: 40×40 pixels with 50% overlap for the 1st set, and 150×150 with 40% overlap for the 2nd set was chosen. The window size was chosen so as to cover the width of one person. Moreover, the size perfectly fits within the maximum movement limit for PIV processing, i.e. movement should be restricted to one-quarter of the window.

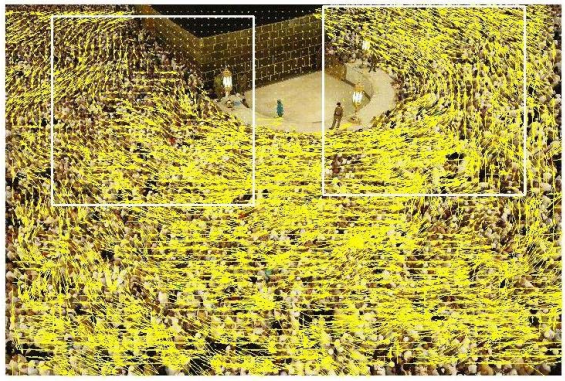

(a)

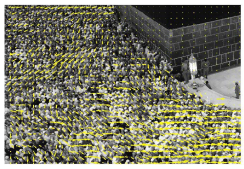

(b)

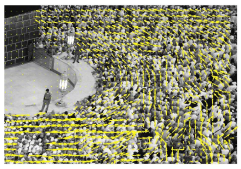

(c)

Fig. 6. Input image and vectors of third dataset. Magnified sections show the direction of left and right sections.

Figure 6 presents one frame of the third test set for PIV processing, together with the velocity vectors. The image resolution was 5760×3840 pixels. The spot size considered was 150×150 with 40% overlap. From the vector plot one can clearly observe the presence of pushing waves in the flow. Such wavy motions are experienced in many high density crowds. It can serve as an indication that accidents are likely. At the bottom of the figure, a zoomed version of the vector plots can be seen. The vectors show the direction of the flow for a smaller portion of the image.

A. Perspective Correction Results

On many occassions, the images captured by CCTV camera may have a high amount of noise in them. Moreover, the camera angle or perspective may also incorporate additional noise to the image-to-world transformation procedure. To get an estimate of this error bound, a set of random points were evaluated to check how much error is incurred with the proposed image-to-world perspective correction scheme. In Table V the accuracy of this transformation process is summarized for four random locations. It can be seen that the maximum amount of error incorporated during the projection corresponds approximately to the width of 3.54 persons.

TABLE V
COMPARISON OF PROJECTED LOCATION VS ACTUAL LOCATION

World x (m)	World y (m)	World z (m)	Projected x (m)	Projected y (m)	Projected z (m)	Error (person width)
1.77	15.35	0.0	2.54	14.65	0.0008	2.08
-1.84	15.40	0.0	-0.183	15.39	0.0008	2.02
5.85	-6.52	0.0	4.09	-6.31	0.0008	3.54
-4.27	5.52	0.0	-4.87	5.18	0.0008	1.37

TABLE VI
AVERAGE PEDESTRIAN VELOCITY

Dataset	Speed (m/s)	Uncertainty
1	0.375	0.0624
2	0.245	0.0289
3	0.2375	0.0113

TABLE VII
COMPARISON OF PIV TIMING WITH OPTICAL FLOW

Image Size (pixel)	Optical Flow (sec)	PIV (sec)
576x384	51.46	0.0469
288x192	20.26	0.0286
5760x3840	-	2.92

B. Average Velocities

The average velocities after perspective correction and pixel-to-world conversion are presented in Table VI. Along with the velocity magnitude, the uncertainties are also listed. It can be seen that the first set has a high amount of uncertainty, not surprising considering the fact that the images had a high amount of noise. When the average velocity values are compared with other studies of the Hajj [6], [63], the results are found to be in close agreement with them.

C. Compute Time

Another major benefit of extracting pedestrian velocity from PIV is that it is able to produce results in real-time. The compute times for velocity extraction of PIV and optical flow is listed in Table VII. One can see that PIV results are obtained in a significantly lower amount of time compared to the optical flow. The prime reason behind PIV's superior performance is that PIV resolves velocities in per spot size whereas, for optical flow, velocities are resolved for every pixel in the image. Resolving velocities per pixel level may be slightly more accurate. However, considering the demand for real-time extraction of pedestrian velocities from images, the PIV method appears to be a viable alternative.

The timings reported in Table VII were conducted on an Intel Core i5 processor with 8GB RAM. The computer program for PIV written was by the author in C++. No parallelization or performance optimization was performed. For optical flow the implementation of the open source library OpenCV [64], [65] was used. It can be seen that optical flow has not been able to resolve velocities from the full CCTV image. This is because optical flow is currently beyond real-time [66]. To make the comparison complete, lower dimensional image segments were chosen.

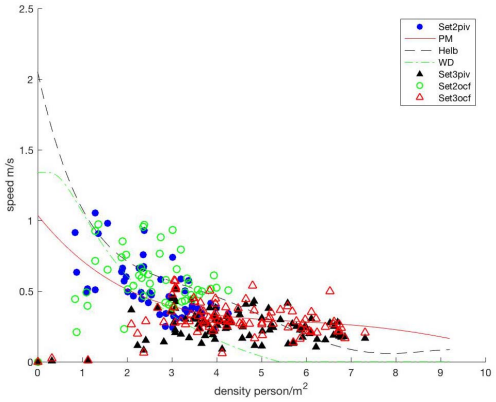

Fig. 7. Fundamental diagram of 1st (blue circles) and 2nd set (black triangles). Optical flow results are presented green hollow circle (set2ocf) for 2nd set and red hollow triangle (set3ocf) for 3rd set. The red line is the Predechenskii curve (PM), the green dotted line is the Wiedmann curve (WD) and the black dotted line is the Helbing curve (Helb).

D. The Fundamental Diagram

The fundamental diagram provides a snapshot of the flow at a particular time. It is a plot of the speed of pedestrians vs. their density in a region or area. The fundamental diagram allows a quick evaluation of the overall conditions of pedestrian flow at a given time. In Figure 7, the fundamental diagram is presented for the 2nd and 3rd set of test images. The densities required for the fundamental were obtained through manual annotations of head counting from images. In the figure the trianglular and circular dots represent the 2nd and 3rd set respectively. Optical flow results are also presented. The filled circles and triangles represent PIV velocity while hollow circles and triangles represent optical flow results. The difference between mean velocities from Optical flow and PIV is 0.075 m/s. Common fundamental diagrams such Predtechenskii and Milinskii [29], Helbing *et al.* [5], and Wiedmann [67] are also shown in the figure and labeled as PM, Helb and WD. Other empirical work of fundamental diagrams for various crowd situations can be found in the works of Seyfried *et al.* [68] and Chattaraj *et al.* [69].

The sporadic nature of crowd flow is clearly evident in the density-velocity relation. One can see a considerable spread of velocities for low densities, as people can move freely at their desired speeds. As density increases, the fluctuation in velocities gets reduced. The same behaviour has been reported by Predtechenskii and Milinskii [29]. In real life, if the pedestrian density information is not readily available, this high dispersion of pedestrian velocities could provide an idea of the approximate level of pedestrian density. Also, since the velocities have followed similar trends of PM, Helb and WD curves, these curves can be taken as a baseline in order to understand the instantaneous nature of the flow.

In order to obtain localized flow properties (density, velocity), the entire image has been divided into 100 smaller cells of same pixel dimensions. There are 10 divisions in the horizontal and vertical directions. A schematic arrangement of the cells can be seen in Figure 8.

Figure 9 shows the local speed distributions. Speed values range from 0.2 to 0.35 m/s.

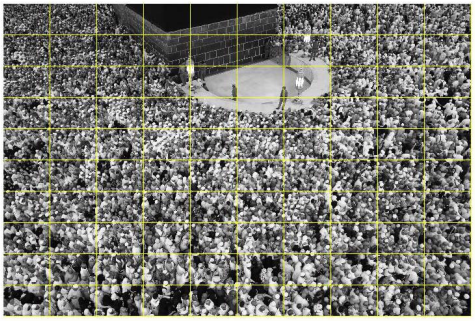

Fig. 8. Schematic arrangement of cells used for perspective correction and fundamental diagram construction.

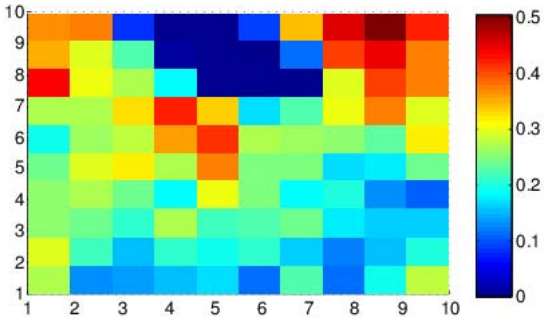

Fig. 9. Local speed distribution for second test set image. Speed distribution is mostly consistent with some areas having little higher velocity than the average.

VI. Conclusions and Outlook

A PIV based framework for automated analysis of high density crowds through CCTV images has been presented, and a qualitative and quantitative analysis on the feasibility of PIV analysis for high density pedestrian flow has been performed. The pixel data from PIV analysis is transformed to real world units following projective geometry. The fundamental diagram has been constructed for a 'real life' high density flow which is rare considering the risks associated with performing experiments with dense crowds. The framework has been tested with images of various resolutions and illuminations. The study was conducted in one location (Mecca) with three different camera angles.

While the results of this automated PIV analysis have been very encouraging, it is too early to make bold conclusions of its widespread applicability in the exploration of high density pedestrian dynamics.

Acknowledgment

The authors would like to acknowledge the help of SL Rasch (Stuttgart, Germany) for the images used for testing the concepts elaborated in this work.

References

[1] J. Baek, J. Kim, and E. Kim, "Fast and efficient pedestrian detection via the cascade implementation of an additive kernel support vector machine," *IEEE Trans. Intell. Transp. Syst.*, vol. 18, no. 4, pp. 902–916, Apr. 2017.

[2] L. Oliveira, U. Nunes, and P. Peixoto, "On exploration of classifier ensemble synergism in pedestrian detection," *IEEE Trans. Intell. Transp. Syst.*, vol. 11, no. 1, pp. 16–27, Mar. 2010.

[3] X. Li *et al.*, "A unified framework for concurrent pedestrian and cyclist detection," *IEEE Trans. Intell. Transp. Syst.*, vol. 18, no. 2, pp. 269–281, Feb. 2017.

[4] A. Johansson, D. Helbing, H. Z. Al-Abideen, and S. Al-Bosta, "From crowd dynamics to crowd safety: A video-based analysis," *Adv. Complex Syst.*, vol. 11, no. 4, pp. 497–527, 2008.

[5] D. Helbing, A. Johansson, and H. Z. Al-Abideen, "Dynamics of crowd disasters: An empirical study," *Phys. Rev. E, Stat. Phys. Plasmas Fluids Relat. Interdiscip. Top.*, vol. 75, no. 4, 2007, Art. no. 046109.

[6] P. Dambalmath, B. Muhammad, E. Haug, and R. Löhner, "Fundamental diagrams for specific very high density crowds," in *Proc. Pedestrian Evacuation Dyn.*, 2016, pp. 6–11.

[7] R. Lohner, B. Muhamad, P. Dambalmath, and E. Haug, "Fundamental diagrams for specific very high density crowds," *Collective Dyn.*, vol. 2, pp. 1–15, Jan. 2018.

[8] B. K. P. Horn and B. G. Schunck, "Determining optical flow," *Artif. Intell.*, vol. 17, nos. 1–3, pp. 185–204, 1981.

[9] B. D. Lucas and T. Kanade, "An iterative image registration technique with an application to stereo vision," in *Proc. Int. Joint Conf. Artif. Intell.*, 1981, pp. 674–679.

[10] W. Jiayue, W. Wenguo, and Z. Xiaole, "Comparison of turbulent pedestrian behaviors between Mina and Love parade," *Procedia Eng.*, vol. 84, pp. 708–714, Jan. 2014.

[11] J. Ma, W. Song, S. M. Lo, and Z. Fang, "New insights into turbulent pedestrian movement pattern in crowd-quakes," *J. Stat. Mech., Theory Exp.*, vol. 2013, no. 2, 2013, Art. no. P02028.

[12] X. L. Zhang, W. G. Weng, and H. Y. Yuan, "Empirical study of crowd behavior during a real mass event," *J. Stat. Mech., Theory Exp.*, vol. 2012, no. 8, 2012, Art. no. P08012.

[13] R. Adrian and C. Yao, "Development of pulsed laser velocimetry (PLV) for measurement of turbulent flow," in *Proc. Symp. Turbulence*, 1984, pp. 170–184.

[14] R. J. Adrian, "Particle-imaging techniques for experimental fluid mechanics," *Annu. Rev. Fluid Mech.*, vol. 23, pp. 260–304, Jan. 1991.

[15] C. E. Willert and M. Gharib, "Digital particle image velocimetry," *Exp. Fluids*, vol. 10, no. 4, pp. 181–193, Jan. 1991.

[16] R. D. Keane and R. J. Adrian, "Optimization of particle image velocimeters. I. Double pulsed systems," *Meas. Sci. Technol.*, vol. 11, no. 1, pp. 1202–1215, 1990.

[17] M. S. Soloff, R. J. Adrian, and Z. Liu, "Distortion compensation for generalized stereoscopic particle image velocimetry," *Meas. Sci. Technol.*, vol. 8, no. 12, pp. 1441–1454, 1997.

[18] S. Wereley and C. Meinhart, "Second-order accurate particle image velocimetry," *Exp. Fluids*, vol. 31, no. 3, pp. 258–268, 2001.

[19] F. Scarano, "Iterative image deformation methods in PIV," *Meas. Sci. Technol.*, vol. 13, no. 1, pp. R1–R19, 2002.

[20] M. Thomas, S. Misra, C. Kambhamettu, and J. T. Kirby, "A robust motion estimation algorithm for PIV," *Meas. Sci. Technol.*, vol. 16, no. 3, pp. 865–877, 2005.

[21] M. Baqui and Z. Mahmud, "Experimental characterization of an integrated flow separation control device," M.S. thesis, North Dakota State Univ., Fargo, ND, USA, 2010.

[22] M. Baqui and Z. Mahmud, "Experimental characterization of an integrated flow control method with blowing and DBD plasma actuator," in *Proc. 41st AIAA Fluid Dyn. Conf. Exhib.*, 2011, p. 3095.

[23] S. Vanlanduit, J. Vanherzeele, R. Longo, and P. Guillaume, "A digital image correlation method for fatigue test experiments," *Opt. Lasers Eng.*, vol. 47, no. 3, pp. 371–378, 2009.

[24] E. A. Cowen and J. K. Sveen, "Quantitative imaging techniques and their application to wavy flows," in *PIV and Water Waves*. Singapore: World Scientific, 2004.

[25] M. Rossi, E. Esposito, and E. P. Tomasini, "PIV application to fluid dynamics of bass reflex ports," in *Particle Image Velocimetry*. Berlin, Germany: Springer, 2007, pp. 259–270.

[26] W. Thielicke and E. J. Stamhuis. (2014). *PIVlab—Time-Resolved Digital Particle Image Velocimetry Tool for MATLAB (Version: 1.41)*. [Online]. Available: http://dx.doi.org/10.6084/m9.figshare.1092508

[27] J. Sveen. (1999). *MatPIV—A Free MATLAB-Toolbox for Particle Image Velocimetry. (Version: 1.7)*. [Online]. Available: https://www.mn.uio.no/math/english/people/aca/jks/matpiv/

[28] Z. J. Taylor, R. Gurka, G. A. Kopp, and A. Liberzon, "Long-duration time-resolved PIV to study unsteady aerodynamics," *IEEE Trans. Instrum. Meas.*, vol. 59, no. 12, pp. 3262–3269, Dec. 2010.

[29] V. Predtechenskii and A. Milinskii, "Planning for foot traffic flow in buildings," U.S. Dept. Commerce, Nat. Sci. Found., New Delhi, India, Tech. Rep., 1978.

[30] J. J. Fruin and G. R. Strakosch, *Pedestrian Planning and Design*. New York, NY, USA: Metropolitan Association of Urban Designers and Environmental Planners, 1971.

[31] A. Schadschneider, W. Klingsch, H. Klüpfel, T. Kretz, C. Rogsch, and A. Seyfried, "Evacuation dynamics: Empirical results, modeling and applications," in *Encyclopedia of Complexity and Systems Science*. New York, NY, USA: Springer, 2009, pp. 3142–3176.

[32] T. Kretz, A. Grünebohm, M. Kaufman, F. Mazur, and M. Schreckenberg, "Experimental study of pedestrian counterflow in a corridor," *J. Stat. Mech., Theory Exp.*, vol. 2006, no. 10, 2006, Art. no. P10001.

[33] D. Helbing, A. J. L. Buzna, and T. Werner, "Self-organized pedestrian crowd dynamics: Experiments, simulations, and design solutions," *Transp. Sci.*, vol. 39, no. 1, pp. 1–24, 2005.

[34] A. Seyfried, B. Steffen, and T. Lippert, "Basics of modelling the pedestrian flow," *Phys. A, Stat. Mech. Appl.*, vol. 368, no. 1, pp. 232–238, 2006.

[35] M. Isobe, T. Adachi, and T. Nagatani, "Experiment and simulation of pedestrian counter flow," *Phys. A, Stat. Mech. Appl.*, vol. 336, pp. 638–650, May 2004.

[36] A. Jelić, C. Appert-Rolland, S. Lemercier, and J. Pettré, "Properties of pedestrians walking in line: Fundamental diagrams," *Phys. Rev. E, Stat. Phys. Plasmas Fluids Relat. Interdiscip. Top.*, vol. 3, Mar. 2012, Art. no. 036111.

[37] M. Boltes, S. Holl, A. Tordeux, A. Seyfried, A. Schadschneider, and U. Lang, "Influences of extraction techniques on the quality of measured quantities of pedestrian characteristics," Jülich Supercomput. Center, Jülich, Germany, Tech. Rep., 2016. [Online]. Available: http://hdl.handle.net/2128/13080

[38] V. Ziemer, A. Seyfried, and A. Schadschneider, "Congestion dynamics in pedestrian single-file motion," in *Traffic and Granular Flow*. Cham, Switzerland: Springer, 2016, pp. 89–96.

[39] Y. Yuan, W. Daamen, D. Duives, and S. Hoogendoorn, "Comparison of three algorithms for real-time pedestrian state estimation-supporting a monitoring dashboard for large-scale events," in *Proc. IEEE 19th Int. Conf. Intell. Transp. Syst. (ITSC)*, Nov. 2016, pp. 2601–2606.

[40] W. Daamen, *Modelling Passenger Flows in Public Transport Facilities*. Deflt, The Netherlands: DUP Science, 2004.

[41] S. P. Hoogendoorn, W. Daamen, and P. H. L. Bovy, "Extracting microscopic pedestrian characteristics from video data," in *Proc. Transp. Res. Board Annu. Meeting*, 2003, pp. 1–15.

[42] S. D. Khan, G. Vizzari, and S. Bandini, "Identifying sources and sinks and detecting dominant motion patterns in crowds," *Transp. Res. Procedia*, vol. 2, pp. 195–200, Jan. 2014.

[43] D. Ettehadieh, B. Farooq, and N. Saunier, "Automated pedestrian data-collection and flow analysis in public spaces," *Transp. Res. Procedia*, vol. 2, pp. 207–212, Jan. 2014.

[44] A. Corbetta, J. Meeusen, C.-M. Lee, and F. Toschi, "Continuous measurements of real-life bidirectional pedestrian flows on a wide walkway," in *Proc. Pedestrian Evacuation Dyn.*, 2016, pp. 18–25.

[45] P. Zhao, L. Sun, L. Cui, W. Luo, and Y. Ding, "The walking behaviours of pedestrian social group in the corridor of subway station," in *Proc. Pedestrian Evacuation Dyn.*, 2016, pp. 34–41.

[46] C. Kogler, S. Seer, and N. Brandle, "Eight years of good flux: Long-term performance evaluation of an automatic crowd management system for public transport," in *Proc. Pedestrian Evacuation Dyn.*, 2016, pp. 69–75.

[47] H. Klüpfel, "The simulation of crowd dynamics at very large events—Calibration, empirical data, and validation," in *Proc. Pedestrian Evacuation Dyn.*, 2005, pp. 285–296.

[48] H. Idrees, I. Saleemi, C. Seibert, and M. Shah, "Multi-source multi-scale counting in extremely dense crowd images," in *Proc. IEEE Conf. Comput. Vis. Pattern Recognit.*, Jun. 2013, pp. 2547–2554.

[49] W. Ge and R. T. Collins, "Marked point processes for crowd counting," in *Proc. IEEE Conf. Comput. Vis. Pattern Recognit. (CVPR)*, Jun. 2009, pp. 2913–2920.

[50] A. Johansson, D. Helbing, H. Al-Abideen, and S. Al-Bosta, "From crowd dynamics to crowd safety: A video-based analysis," *Adv. Complex Syst.*, vol. 11, no. 4, pp. 497–572, 2008.

[51] B. Krausz and C. Bauckhage, "Loveparade 2010: Automatic video analysis of a crowd disaster," *Comput. Vis. Image Understand.*, vol. 116, no. 3, pp. 307–319, 2008.

[52] T. Liu and L. Shen, "Fluid flow and optical flow," *J. Fluid Mech.*, vol. 614, pp. 253–291, Nov. 2008.

[53] T. Ahonen, A. Hadid, and M. Pietikainen, "Face description with local binary patterns: Application to face recognition," *IEEE Trans. Pattern Anal. Mach. Intell.*, vol. 28, no. 12, pp. 2037–2041, Dec. 2006.

[54] M. Baqui and R. Löhner, "Real-time crowd safety and comfort management from CCTV images," *Proc. SPIE*, vol. 10223, May 2017, Art. no. 1022304.

[55] B. H. Timmins, B. W. Wilson, B. L. Smith, and P. P. Vlachos, "A method for automatic estimation of instantaneous local uncertainty in particle image velocimetry measurements," *Exp. Fluids*, vol. 53, no. 4, pp. 1133–1147, 2012.

[56] A. Sciacchitano *et al.*, "Collaborative framework for PIV uncertainty quantification: Comparative assessment of methods," *Meas. Sci. Technol.*, vol. 26, no. 7, 2015, Art. no. 074004.

[57] J. J. Charonko and P. P. Vlachos, "Estimation of uncertainty bounds for individual particle image velocimetry measurements from cross-correlation peak ratio," *Meas. Sci. Technol.*, vol. 24, no. 6, 2013, Art. no. 065301.

[58] Z. Xue, J. J. Charonko, and P. P. Vlachos, "Particle image velocimetry correlation signal-to-noise ratio metrics and measurement uncertainty quantification," *Meas. Sci. Technol.*, vol. 25, no. 11, 2014, Art. no. 115301.

[59] Z. Xue, J. J. Charonko, and P. P. Vlachos, "Signal-to-noise ratio, error and uncertainty of PIV measurement," in *Proc. 10th Int. Symp. Part. Image Velocimetry (PIV)*, Delft, The Netherlands, 2013, pp. 1–18.

[60] A. Sciacchitano, B. Wieneke, and F. Scarano, "PIV uncertainty quantification by image matching," *Meas. Sci. Technol.*, vol. 24, no. 4, 2013, Art. no. 045302.

[61] C. Harris and M. Stephens, "A combined corner and edge detector," in *Proc. 4th Alvey Vis. Conf.*, 1988, pp. 147–151.

[62] B. N. Taylor and C. E. Kuyatt, *Guidelines for Evaluating and Expressing the Uncertainty of NIST Measurement Results*. Gaithersburg, MD, USA: National Institute of Standards and Technology, 1994.

[63] M. H. Dridi, "Tracking individual targets in high density crowd scenes analysis of a video recording in hajj 2009," *Current Urban Stud.*, vol. 3, pp. 35–53, Mar. 2015.

[64] Itseez. (2015). *Open Source Computer Vision Library*. [Online]. Available: https://github.com/itseez/opencv

[65] *The OpenCV Reference Manual*, 2nd ed., Itseez, Apr. 2014. [Online]. Available: https://docs.opencv.org/3.0-beta/

[66] A. Wedel and D. Cremers, *Stereo Scene Flow for 3D Motion Analysis*. London, U.K.: Springer, 2011.

[67] U. Weidmann, "Transporttechnik der fussgänger," Institut für Verkehrsplanung, Transporttechnik, Strassen-und Eisenbahnbau, ETH Zürich, Tech. Rep., 1992. doi: 10.3929/ethz-a-000687810.

[68] A. Seyfried, B. Steffen, W. Klingsch, and M. Boltes, "The fundamental diagram of pedestrian movement revisited," *J. Stat. Mech., Theory Exp.*, vol. 2005, no. 10, 2005, Art. no. P10002.

[69] U. Chattaraj, A. Seyfried, and P. Chakroborty, "Comparison of pedestrian fundamental diagram across cultures," *Adv. Complex Syst.*, vol. 12, no. 3, pp. 393–405, 2009.

Muhammad Baqui received the B.Sc. and M.S. degrees in mechanical engineering and the Ph.D. degree in computational sciences from George Mason University. His research work is focused on understanding high density pedestrian flows through image processing and computational methods.

Rainald Löhner received the M.Sc. degree in mechanical engineering from Technische Universität Braunschweig, Germany, and the Ph.D. and D.Sc. in civil engineering from the University College of Swansea, Wales. He is the Head of the Computational Fluid Dynamics Center, George Mason University. He has authored more than 850 articles in the areas of pedestrian dynamics, high performance computing, computational fluid dynamics, and mesh generation.